Supporting Information

Mechanism of molecular conductance enhanced via the D-A effect

Wei Feng,[a] Tianjiao Hou,[a] Xuerui Li,[a] Wenjie Du,[a] Yunchuan Li, *[a] Zhiye Wang*[b]

AUTHOR ADDRESS.

[a.] The College of Materials Science and Engineering, Wuhan University of Science and Technology, Wuhan 430081, China.

[b.] Department of Mechanical Engineering, Henan University of Engineering, Zhengzhou, 451191, China.

Contents

S1. Synthesis pathway of the target molecule

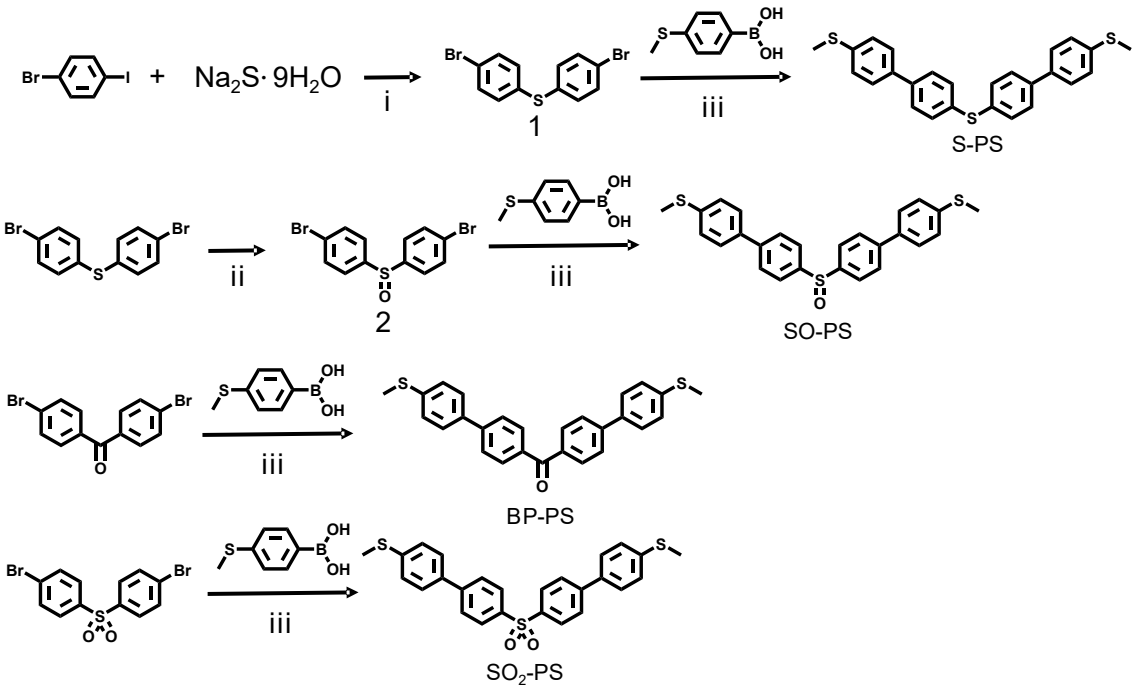

Figure S1. Synthetic routes of the target molecules S-PS, SO-PS, BP-PS and SO_2-PS. i: Cuprous iodide, potassium carbonate, N, N-dimethylformamide; ii: AcOH, dichloromethane, hydrogen peroxide; iii: 2M K_2CO_3 aqueous solution, ethanol, toluene, $Pd_3(PPh_3)_4$.

Compound 1. 1-Bromo-4-iodobenzene (1 g, 3.5 mmol), sodium sulfide nonahydrate (512 mg, 2.13 mmol), copper(I) iodide (29.68 mg), aqueous potassium carbonate solution (477 mg), and N,N-dimethylformamide (15 mL) were added to a three-necked flask, and the reaction mixture was bubbled with N_2 gas for 15 minutes. The suspension was stirred at 120 °C for 8 h under a nitrogen atmosphere. After cooling to room temperature, the mixture was extracted with dichloromethane and dried over magnesium sulfate. The solvent was removed, and the residue was purified by silica gel column chromatography to afford a solid product (601 mg, yield 99%).

S-PS. Compound 1 (600 mg, 1.74 mmol), 4-(methylthio) phenylboronic acid (649 mg, 3.86 mmol), aqueous potassium carbonate solution (3.2 g, 12 mL), toluene (54 mL), ethanol (35 mL), and tetrakis (triphenylphosphine) palladium (70.24 mg) were charged into a three-necked flask, and the reaction mixture was bubbled with N_2 gas

for 15 minutes. The suspension was stirred at 80 °C for 24 h under a nitrogen atmosphere. Upon cooling to room temperature, the mixture was extracted with dichloromethane and dried over anhydrous sodium sulfate. The solvent was evaporated, and the residue was subjected to silica gel column chromatography to give a pale yellow solid (464 mg, yield 64%). ^{1}H NMR (600 MHz, $CDCl_3$) δ 7.53–7.47 (m, 6H), 7.39 (dd, J = 8.2, 2.1 Hz, 4H), 7.34–7.30 (m, 6H), 2.52 (d, J = 6.9 Hz, 6H).

Compound 2. Compound 1 (500 mg, 1.5 mmol), glacial acetic acid (30 mL), dichloromethane (15 mL), and hydrogen peroxide (20 mL) were added to a three-necked flask. The suspension was reacted at room temperature for 2 h. The mixture was extracted with dichloromethane and dried over anhydrous sodium sulfate. The solvent was removed, and the residue was purified by silica gel column chromatography to obtain a pale yellow solid (461 mg, yield 85%).

SO-PS. Compound 1 was replaced with Compound 2 (458 mg, 1.272 mmol), and the reaction was carried out following the same procedure as that for S-PS, affording a yellow solid (227 mg, yield 40%). ^{1}H NMR (600 MHz, $CDCl_3$) δ 7.73 (d, J = 8.4 Hz, 4H), 7.66 (d, J = 8.4 Hz, 4H), 7.49 (d, J = 8.4 Hz, 4H), 7.32 (d, J = 8.4 Hz, 4H), 2.52 (s, 6H).

BP-PS. Compound 1 was replaced with 4,4'-dibromobenzophenone (240 mg, 0.6 mmol), and the same synthetic protocol as that for S-PS was adopted, giving a pale yellow solid (45 mg, yield 17%). ^{1}H NMR (600 MHz, $CDCl_3$) δ 7.91 (d, J = 8.4 Hz, 4H), 7.70 (d, J = 8.4 Hz, 4H), 7.60 (d, J = 8.1 Hz, 4H), 7.36 (d, J = 8.1 Hz, 4H), 2.55 (s, 6H).

SO_2-PS. Compound 1 was replaced with 4,4'-dibromodiphenyl sulfone (752 mg, 2 mmol), and the reaction was performed using the same method as that for S-PS, yielding a pale yellow solid (600 mg, yield 65%). ^{1}H NMR (600 MHz, $CDCl_3$) δ 8.02 (d, J = 8.4 Hz, 4H), 7.69 (d, J = 8.2 Hz, 4H), 7.50 (d, J = 8.4 Hz, 4H), 7.32 (d, J = 8.4 Hz, 4H), 2.52 (s, 6H)

S2. ^{1}H NMR spectra of the target compounds

^{1}H NMR spectrum of S-PS

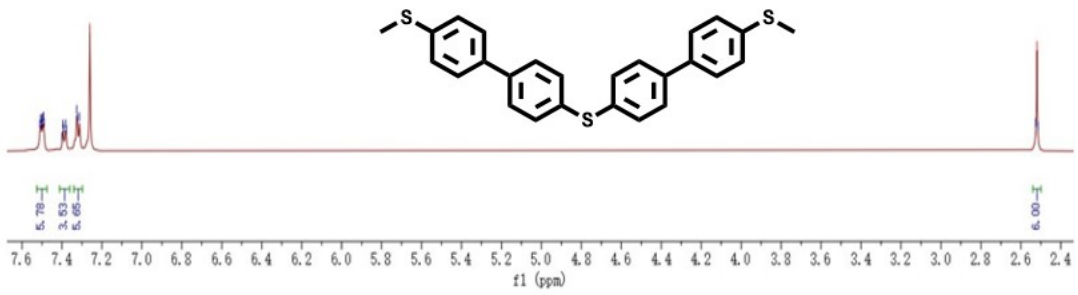

^{1}H NMR spectrum of SO-PS

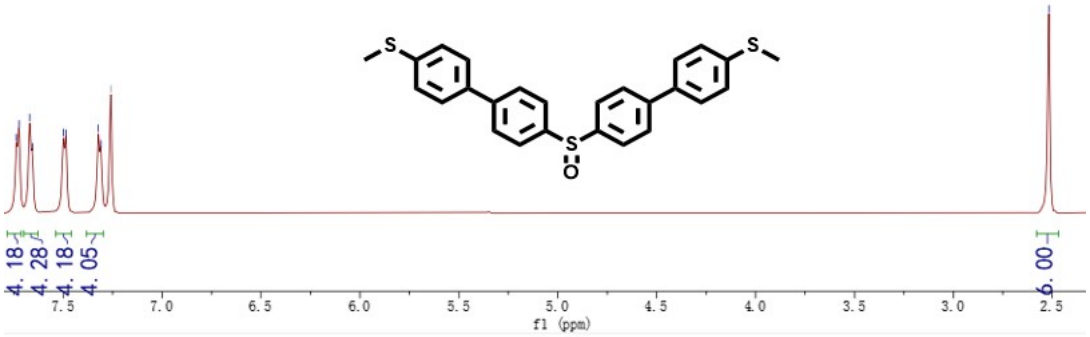

^{1}H NMR spectrum of BP-PS

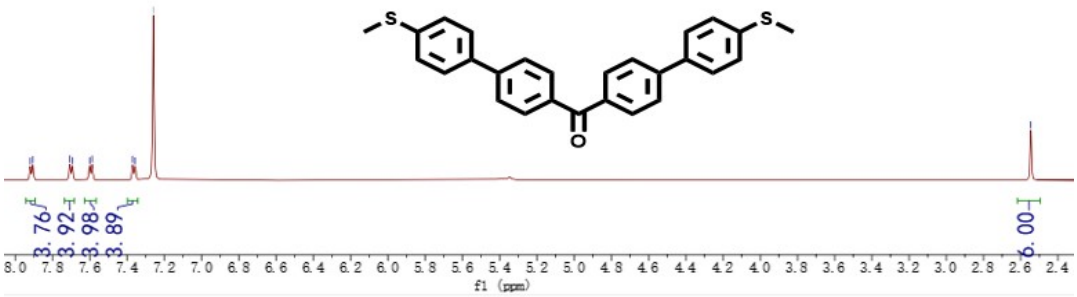

^{1}H NMR spectrum of SO_2-PS

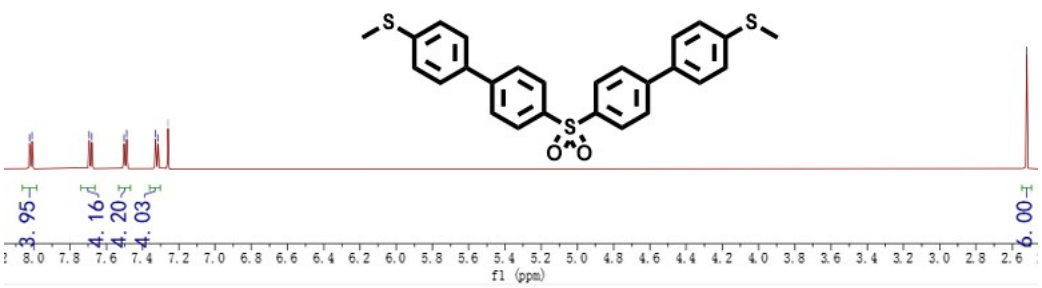

S3. Home-built STM setup[1]

Experiments were conducted using a home-built scanning tunneling microscope (STM) system. The gold tip was brought into contact with and retracted from the substrate using a stepping piezomotor (Newport 8742-4-KIT, Germany), which provided a positioning resolution of 0.03 nm. This piezomotor was driven by a uniaxial piezoelectric actuator (Piezosystem Jena S-303.0L, Germany). Current signals were acquired via an NI PXIe-4309 data acquisition module (18-bit resolution, 2 MS/s per channel) and amplified by a variable-gain current-to-voltage (I-V) converter (DLPCA-200, Femto, Germany). The entire system, integrating hardware control and data acquisition, was operated by a custom-developed LabVIEW program.

Single-Molecule Conductance Measurement: Target molecules were dissolved in 1,2,4-trichlorobenzene (TCB) to a concentration of a 1 mM. During measurements, 20 μL of the molecule-containing solution was deposited onto the gold substrate. Conductance tests were performed at room temperature via the scanning tunneling microscope break junction (STM-BJ) technique. This method involves piezoelectric control of a nanoscale gold tip to approach a gold substrate, followed by retraction to form a nanogap. As the nanogap continuously expands, target molecules spontaneously bridge the probe and substrate via thermal motion, forming a single-molecule junction that completes an electrical circuit-enabling conductance measurement of the captured molecule. By repeating this process for thousands of times, current signals were recorded in real time as a function of the distance between two nanoelectrodes. Throughout the entire measurement process, a bias voltage of 0.1 V was applied to the substrate, the gold tip was moved at a speed of 20 nm/s. The signal amplification factor was set to 10^7 V/A, and signals were acquired at a sampling rate of 20 kHz.

S4. DFT-optimized structure

The geometric optimization of the target molecule was performed using the B3LYP/6-31 G(d,p) basis set and functional.[2,3]

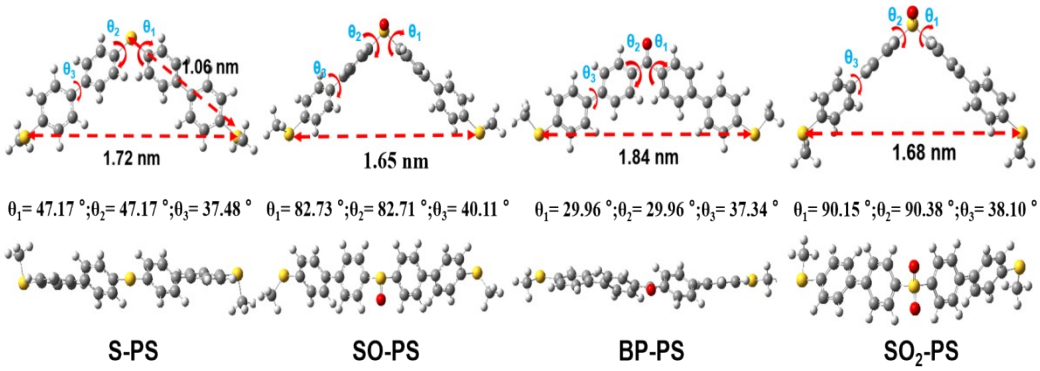

Figure S2. Schematic diagrams of molecular structures with dihedral angles of S-PS, SO-PS, BP-PS, and SO_2-PS showed.

The measured molecular bond lengths in the text are as follows: 0.49 ± 0.11 nm for S-PS, 1.06 ± 0.13 nm for SO-PS, 1.27 ± 0.17 nm for BP-PS, and 1.16 ± 0.13 nm for SO_2-PS. After accounting for the snap-back distance of the gold electrodes (0.5 nm), the corresponding molecular junction lengths are determined to be: 0.99 ± 0.11 nm for S-PS, 1.56 ± 0.13 nm for SO-PS, 1.77 ± 0.17 nm for BP-PS, and 1.66 ± 0.13 nm for SO_2-PS. Comparison with the optimized molecular geometries suggests that the S-PS junction is likely formed via partial incorporation of the molecule, with the central disulfide S—a relatively strong anchoring motif—participating in the binding. In contrast, SO-PS, BP-PS, and SO_2-PS predominantly anchor between the two gold electrodes through the terminal sulfur atoms at both ends.

S5. Molecular junction geometries

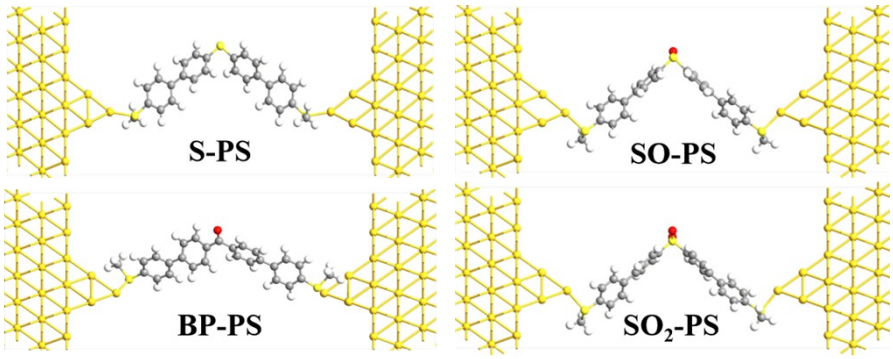

Figure S3. Molecular junction configurations of S-PS, SO-PS, BP-PS, and SO_2-PS adopted in the first-principles transport calculations.

S6. Ultraviolet-Visible absorption spectroscopy (UV) and Cyclic voltammetry (CV) for target molecules

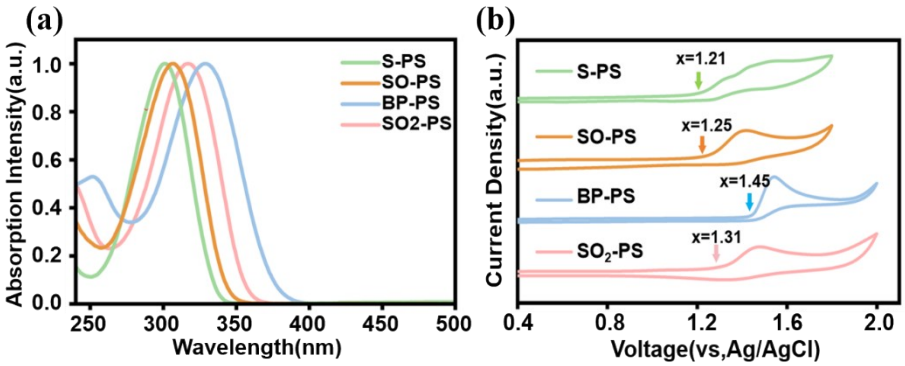

Figure S4. (a) Ultraviolet-Visible absorption spectroscopy and (b) Cyclic voltammetry results of S-PS, SO-PS, BP-PS, and SO_2-PS.

Table S1. A summary of molecular orbital energy level data obtained via ultraviolet-visible absorption threshold and the onset of oxidation potentials.

Molecule	Eox (V)	λ_{abs}(nm)	HOMO (eV)	LUMO (eV)	E_g (eV)
S-PS	1.21	301	- 5.48	- 1.36	4.12
SO-PS	1.25	306	- 5.52	- 1.47	4.05
BP-PS	1.45	328.7	- 5.72	- 1.95	3.77
SO_2-PS	1.31	317	- 5.58	- 1.67	3.91

Herein, E_g is the optical bandgap which is calculated by $E_g = 1240 / \lambda_{abs}$ eV (λ_{abs} is the position of the absorption edge in the absorption spectrum, **Figure S3a**). As indicated in CV curve (**Figure S3b**), E_{ox} is the oxidation potential of a molecule. Then, the HOMO is calculated according to the formula[4]: $E_{HOMO} = - (E_{ox} + 4.8 - E_{Fc/Fe+})$ eV, where $E_{Fc/Fe+}$ is measured to be 0.53 V under the same condition. The LUMO level is referred from the relation of $E_{LUMO} = E_{HOMO} + E_g$. The electrochemical measurements were performed under the following conditions. The working electrode for the electrochemical experiment is a gold plate electrode, the counter electrode is a

platinum wire, the reference electrode is a silver/ silver chloride reference electrode, the supporting electrolyte is 72 mM tetrabutylammonium hexafluorophosphate, the solvent is anhydrous dichloromethane, the scan rate is 50 millivolts per second, and the test temperature is room temperature

7. Steady-state Fluorescence Emission Testing

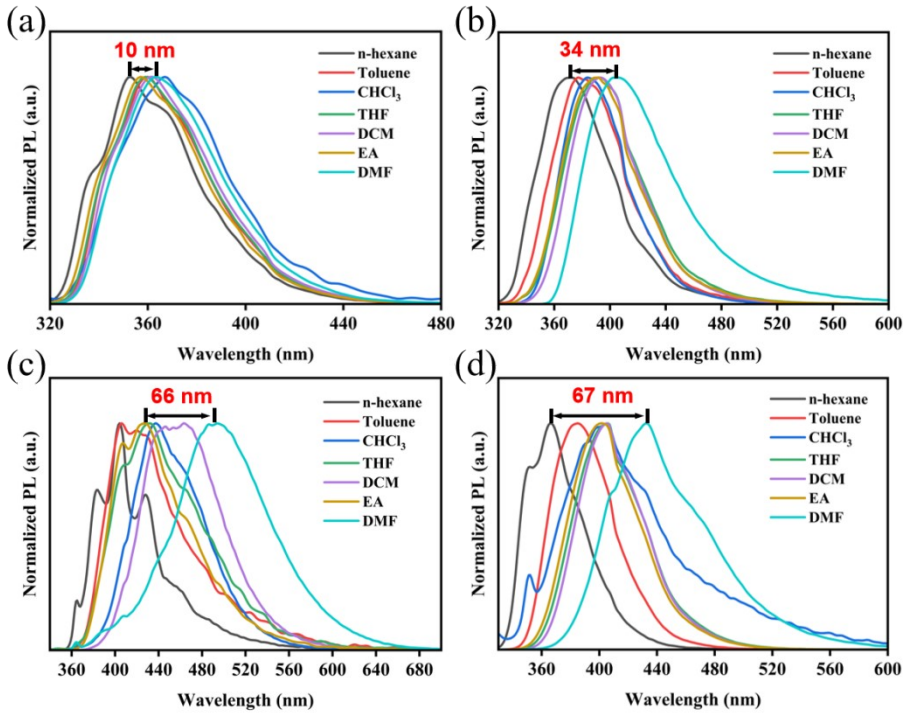

Figure S5. Steady-state fluorescence emission diagrams of S-PS (a), SO-PS (b), BP-PS(c), and SO_2-PS(d). Solvent abbreviations: THF (tetrahydrofuran), DCM (dichloromethane), EA (ethyl acetate), DMF (N,N-dimethylformamide).

S8. Lippert-Mataga Calculation[5]

To determine the change in dipole moment Δμ during excitation, the Stokes shift is expressed as a function of the solvent polarity parameter Δf (ε, n) using the Lippert-Mataga equation (1).

$$hc(\nu_a-\nu_f) = hc(\nu_a^0 - \nu_f^0) - \frac{2(\mu_e - \mu_g)^2}{a^3} f(\epsilon,n) \quad (1),$$

The Stokes shift ($\nu_a - \nu_f$) is related to the solvent's orientational polarizability (f) through the Lippert-Mataga equation. In this context, μ_e and μ_g are the dipole moments in the excited and ground states, respectively, and a is the Onsager cavity radius of the solute molecule. The solvent's dielectric constant and refractive index are denoted by ε and n, respectively. The function $f(\varepsilon, n)$ and the cavity radius a are calculated as follows:

$$f(\epsilon,n) = \frac{\epsilon - 1}{2\epsilon + 1} - \frac{n^2 - 1}{2n^2 - 1} \quad (2),$$

$$a = \left(\frac{3M}{4\Pi Nd}\right)^{1/3} \quad (3),$$

Through the analysis of the fitting curve in highly polar solvents, we obtained the slope value of the fitting line. The ground-state dipole moment μg values of S-PS, SO-PS, BP-PS, and SO_2-PS were estimated respectively by long-range modified density functional theory (DFT) calculation (using the B3LYP/6-31 G (d,p) basis set), which were 0.18, 4.5, 0.92, and 4.81 D, respectively.

Table S2. Detailed positions of absorption and emission peaks in different solvents (data marked in red were not included in the fitting). Solvent abbreviations: THF (tetrahydrofuran), DCM(dichloromethane), EA (ethyl acetate), DMF (N,N-dimethylformamide).

solvent	$\Delta f(\varepsilon,n)$	S-PS			SO-PS		
		V_a	V_f	$\Delta\nu(V_a-V_f)$	V_a	V_f	$\Delta\nu(V_a-V_f)$
Hexane	0.0012	301	353	4893.979	306	372	5798.018
toluene	0.014	301	360	5444.813	306	377	6154.539
chloroform	0.147	301	367	5974.635	306	384	6638.072
THF	0.210	301	359	5367.438	306	392	7169.534

EA	0.200	301	357	5211.387	306	393	7234.446
DCM	0.217	301	361	5521.760	306	391	7104.291
DMF	0.276	301	363	5674.382	306	406	8049.196

solvent	$\Delta f(\varepsilon,n)$	**BP-PS**			**SO_2-PS**		
		V_a	V_f	$\Delta\nu\,(V_a-V_f)$	V_a	V_f	$\Delta\nu\,(V_a-V_f)$
Hexane	0.0012	328.7	428	7058.392	317	366	4223.337
toluene	0.014	328.7	406	5792.336	317	385	5571.715
chloroform	0.147	328.7	437	7539.583	317	405	6854.383
THF	0.210	328.7	432	7274.730	317	406	6915.199
EA	0.200	328.7	463	8824.606	317	401	6608.085
DCM	0.217	328.7	427	7003.674	317	405	6854.383
DMF	0.276	328.7	428	7058.392	317	366	4223.337

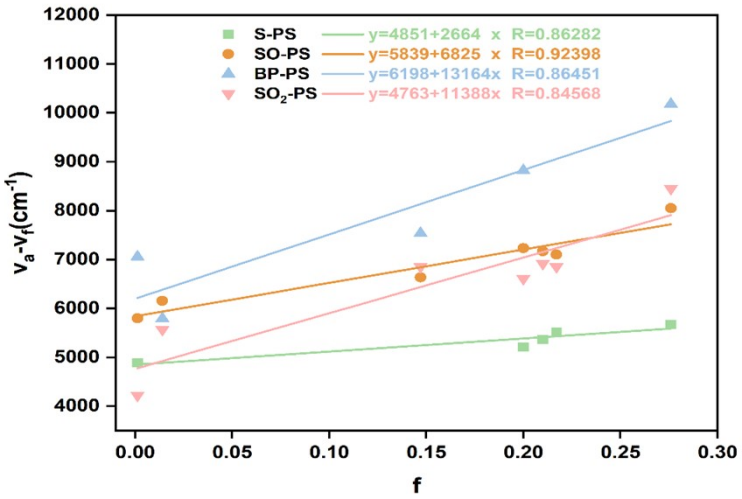

Figure S6. Linear correlation between the orientation polarization intensity (Δf (ε, n)) and Stokes shift ($\nu_a - \nu_f$) for seven solvent: S-PS, SO-PS, BP-PS, and SO_2-PS.

Table S3. Summary of Dipole Moments.

Molecule	μ_e	μ_g	μ_e-μ_g
S-PS	6.91 D	0.18 D	6.73 D
SO-PS	15.44 D	4.50 D	10.94 D
BP-PS	15.78 D	0.92 D	14.86 D
SO_2-PS	22.17 D	7.81 D	14.36 D

Reference:

[1] Huang, M. Z.; Dong, J. Q.; Wang, Z. Y.; Li, Y. C.; Yu, L.; Liu, Y. C.; Qian, G. M.; Chang, S. Revealing the electronic structure of organic emitting semiconductors at the single-molecule level. Chem. Commun. 2020, 56, 14789-14792.

[2] Bourass, M.; Benjelloun, A. T.; Benzakour, M.; Mcharfi, M.; Hamidi, M.; Bouzzine, S. M.; Bouachrine, M. DFT and TD-DFT calculation of new thienopyrazine-based small molecules for organic solar cells. Chem. Cent. J. 2016, 10 (67), 1-11.

[3] Wang, Z. Y.; Huang, M. Z.; Dong, J. Q.; Wang, X.; Li, Y. C.; Sun, M. J.; Chang, S. Utilizing noncovalent conformational locks to create through-space charge transport. J. Phys. Chem. C 2023, 127 (5), 2518-2523.

[4] Huang, S. R.; Chen, L.; Liao, Z. H.; An, Y. K.; Xie, Q.; Huang, B.; Chen, Y. W. Bithiazole-based copolymer with deep HOMO level and noncovalent conformational lock for organic photovoltaics. Org. Electron. 2019, 64, 110-116.

[5] Li, Y. C.; Wang, Z. H.; Li, X. L.; Xie, G. Z.; Chen, D. C.; Wang, Y. F.; Lo, C. C.; Lien, A.; Peng, J. B.; Cao, S.; Su, S. J. Highly Efficient Spiro[fluorene-9,9′-thioxanthene] Core Derived Blue Emitters and Fluorescent/Phosphorescent Hybrid White Organic Light-Emitting Diodes. Chem. Mater. 2015, 27 (3), 1100-1109.